Influence of defects on the absorption edge of InN thin films: The band gap value

J. S. Thakur,[1,*] Y. V. Danylyuk,[1] D. Haddad,[2] V. M. Naik,[3] R. Naik,[2] and G. W. Auner[1]
[1]*Department of Electrical and Computer Engineering, Wayne State University, Detroit, Michigan 48202, USA*
[2]*Department of Physics and Astronomy, Wayne State University, Detroit, Michigan 48201, USA*
[3]*Department of Natural Sciences, University of Michigan-Dearborn, Dearborn, Michigan 48128, USA*
(Received 3 May 2006; revised manuscript received 15 May 2007; published 9 July 2007)

We investigate the optical-absorption spectra of InN thin films whose electron density varies from $\sim 10^{17}$ to $\sim 10^{21}$ cm^{-3}. The low-density films are grown by molecular-beam-epitaxy deposition while highly degenerate films are grown by plasma-source molecular-beam epitaxy. The optical-absorption edge is found to increase from 0.61 to 1.90 eV as the carrier density of the films is increased from low to high density. Since films are polycrystalline and contain various types of defects, we discuss the band gap values by studying the influence of electron degeneracy, electron-electron, electron-ionized impurities, and electron-LO-phonon interaction self-energies on the spectral absorption coefficients of these films. The quasiparticle self-energies of the valence and conduction bands are calculated using dielectric screening within the random-phase approximation. Using one-particle Green's function analysis, we self-consistently determine the chemical potential for films by coupling equations for the chemical potential and the single-particle scattering rate calculated within the effective-mass approximation for the electron scatterings from ionized impurities and LO phonons. By subtracting the influence of self-energies and chemical potential from the optical-absorption edge energy, we estimate the intrinsic band gap values for the films. We also determine the variations in the calculated band gap values due to the variations in the electron effective mass and static dielectric constant. For the lowest-density film, the estimated band gap energy is ~ 0.59 eV, while for the highest-density film, it varies from ~ 0.60 to ~ 0.68 eV depending on the values of electron effective mass and dielectric constant.

DOI: 10.1103/PhysRevB.76.035309 PACS number(s): 78.66.Fd, 63.20.−e, 78.30.−j, 78.20.−e

I. INTRODUCTION

Over the past few years, InN thin films have been extensively investigated for their optical,[1–5] electrical transport,[5–8] and other properties. There are two main reasons driving these investigations. First, films of InN semiconductors are potential candidates for optoelectronic, high-temperature, and high-power electronic device applications. Second, many of the experimental observations are not yet well understood and some are, in fact, controversial.[9–18] This is due to the fact that the fabrication of single crystal InN films has been a challenge[19] because of its stoichiometric instability and low dissociation temperature. Hence, most of the films contain unknown types and amounts of defects[7,8]—randomly distributed charged (positively and/or negatively) impurities, charged states, charge dislocation lines, grain boundaries (in polycrystalline films), surface-charge defects, etc.—manifested through unexpected behavior observed in optical and transport properties.

The presence of the defects is also responsible for new phenomena in these films. For example, donor-type resonant surface defect states lead to the accumulation of electrons on InN surfaces,[20] forming an intrinsic two-dimensional electron gas confined to a very small depth of the surface. These donor-type surface states are, in fact, also predicted by *ab initio* calculations.[21] Because of the polar nature of the wurtzite-crystal structures of these films, the electron interaction with longitudinal optical (LO) phonons is expected to be strong. As a result, coupled modes should be formed in InN films just as seen in other members of the group-III-nitride family, e.g., in GaN films.[22] However, such coupled electron-LO modes have not yet been established[23,24] in InN films. InN films are also known to break down the band gap common cation rule: that the value of the band gap increases as the atomic number decreases. This has been explained in terms of atomic-orbital energies and the band gap deformation potentials.[25]

The low values of mobility[8] (<50 cm^2/V s) in strongly degenerate films clearly demonstrate the presence of a large number of defects. High values of carrier density ($\sim 10^{20}$ cm^{-3}) also suggest a large concentration of donors. In addition to the charged donors, a variety of other defects, such as charge dislocation lines,[26] grain boundaries[27] (in polycrystalline films), and surface-charge defects,[20] is also observed in these films. The presence of these defects is known to influence a wide range of optical and other properties, including the interpreted band gap value—one of the crucial parameters for optical device applications. Many experiments have recently reported a band gap value of InN films that is much smaller[2,15–18] (0.60–0.75 eV) than ~ 1.9 eV, the value that had been established[9–14] for many years. It is generally believed that the smaller values are due to higher quality of films fabricated by improved growth techniques. The films showing large values for their band gap are mostly degenerate, with carrier density in the range of $\sim 10^{20}$ cm^{-3}, and contain a large number of defects.

Recent Mie experiments[18] have shown that the smaller value observed for the band gap is due to the presence of metallic In clusters in the films, which can cause a strong emission around 0.7 eV owing to the surface states at the metal-InN interfaces. The main argument of this work focuses on the absorption edge of a molecular-beam-epitaxy (MBE) sample using thermally detected optical-absorption (TDOA) at very low temperature. The band gap energy in the

 ©2007 The American Physical Society

TDOA spectrum corresponds to the kink located at the meeting point of constant and sloping components, which occurs around 1.4 eV. However, Bechstedt *et al.*[28] argued that the steep increase in the line shape of the dielectric function is very characteristic of InN films observed both experimentally and theoretically and cannot be accepted as definitive of the fundamental gap. Bechstedt *et al.*[28] also argue that in the effective-medium theory of Shubina *et al.*[18] to simulate the absorption line shape, the assumption of an absorption threshold of 2.4 eV for the InN host material is inconsistent with the conclusion of that paper. Later on, Shubina *et al.*[29] showed that the theoretical band structure of InN cannot be invoked as an objection because its output strongly depends on the model used, and the arguments of Bechstedt *et al.*[28] do not contradict their Mie resonance results. Uncertainty still exists in the band gap value of pure InN films.

In addition to experimental investigations of the band gap, there have been numerous attempts to understand the electronic properties of this material using first-principles calculations.[30–32] Within this approach, Persson *et al.*[30] observed that the band structure depends strongly on the exchange-correlation potential: it even becomes metallic if one employs the Perdew-Wang form for the exchange-correlation potential. On the other hand, using the exchange-correlation potential form of Engel and Vosko, the system becomes semiconducting but the band gap value is underestimated (it is around 0.36 eV) for the InN wurtzite structure. Combining local-density approximation with the scissors-operator approximation, the band gap value increases to 0.7 eV agreeing with many of the recent experimental values.

Experimentally, estimation of the band gap value is based on the spectra of the optical-absorption coefficient, $\alpha(\hbar\omega)$, and on photoluminescence measurements.[15,18] Both these measurements are strongly affected by the presence of defects and value of carrier density N_e. To determine the intrinsic value of the band gap for InN films, it is important to extract the influence of defects and carrier density from the optical measurements. The band gap value basically measures the energy needed to create an electron-hole pair; here, an electron is removed from the valence band and placed in an empty state of the conduction band. The energies of electron and hole in their respective bands depend on electron-electron, hole-hole, electron-hole, electron defects, and all other possible interactions which an electron and hole can feel. The magnitudes of these interactions grow both with N_e and number of defects. The interaction energies influence the optical-absorption processes and thus affect the band gap value as observed.

In addition, the presence of defects can also introduce band tailing,[33] further shrinking the effective band gap. Electron-defect interactions renormalize the quasiparticle energy dispersion and thus modify the density of states.[34,35] In *n*-type films, the presence of defects which are predominantly of donor type also elevates the chemical potential because of the increased carrier density. Although these two processes—renormalization of carrier energies[36] and the increase in chemical potential—tend to counteract each another, a significant blueshift can occur in the absorption edge at higher donor concentrations. The band tailing effect basically represents the availability of states in the normally "forbidden" band gap region. This is usually small compared to the shift in chemical potential with electron density—the so-called Moss-Burstein shift.[37]

The overall result of the competing effects, therefore, is that an increase in carrier density leads to an increase in the absorption edge. For free electrons, the chemical potential can be estimated from the Fermi energy provided the level of defects and the temperature are small. In that case, the chemical potential is equal to Fermi energy. However, when the temperature of the electron gas increases, even for high density and defect-free systems, the chemical potential becomes smaller than the Fermi energy. When other interaction effects are also present, the chemical potential decreases even more. Hence, for an accurate estimation of the absorption edge, the chemical-potential contribution due to the electron-defect interaction must also be known.

In this paper, we investigate the contributions from chemical potential and electron interactions with charged impurities and LO phonons to the experimentally observed optical-absorption edge of InN films having a wide range of carrier density. We compute both the self-energy and band tailing contributions for different levels of impurity concentrations in the InN films. Once they are accounted for, an estimate of the intrinsic band gap is possible. Screening by carriers suppresses the electron-charged impurities and LO-phonon interaction energies, thus affecting the density of states (DOS) and chemical-potential values. We therefore also include this self-consistent mechanism in our calculation. The scattering rate required for the determination of DOS is calculated using mass-shell approximation. All the measurements and calculations are done at room temperature.

We begin by reviewing, in Sec. II, the results of measurements on our chosen range of InN thin-film samples. Next, in Sec. III, we discuss a method for self-energy calculation, and a systematic procedure for calculating electron-charged impurities and LO-phonon interactions and chemical potential in a self-consistent manner, including the important screening effects. At the end of Sec. III, we provide our numerical results for the chemical potential as a function of impurity density N_i and for the intrinsic band gap values for different InN films. Finally, we sum up our findings in Sec. IV.

II. EXPERIMENTS AND RESULTS

The InN films used in this study were grown at ~470 °C by MBE at Cornell University[16] and by plasma-source molecular-beam epitaxy (PSMBE) at Wayne State University (WSU).[38,39] Both the PSMBE and MBE samples were grown on *c*-plane sapphire substrates, except that in the MBE samples, there is an additional buffer-layer structure consisting of ~200 nm thick GaN on 10 nm thick AlN. The MBE-grown samples were 0.5–7.5 μm thick with electron mobility[8] ranging from ~900 to 1300 cm^2/V s and were of lower carrier concentration ($N_e < 10^{19}$ cm^{-3}) compared to the WSU samples where $N_e > 10^{20}$ cm^{-3} and the electron mobility ranged between ~15 and 100 cm^2/V s. Films grown at WSU were comparatively thinner, having a typical thickness ~0.5 μm. The carrier densities of these films are determined with the Hall measurements using the Van der Pauw method.

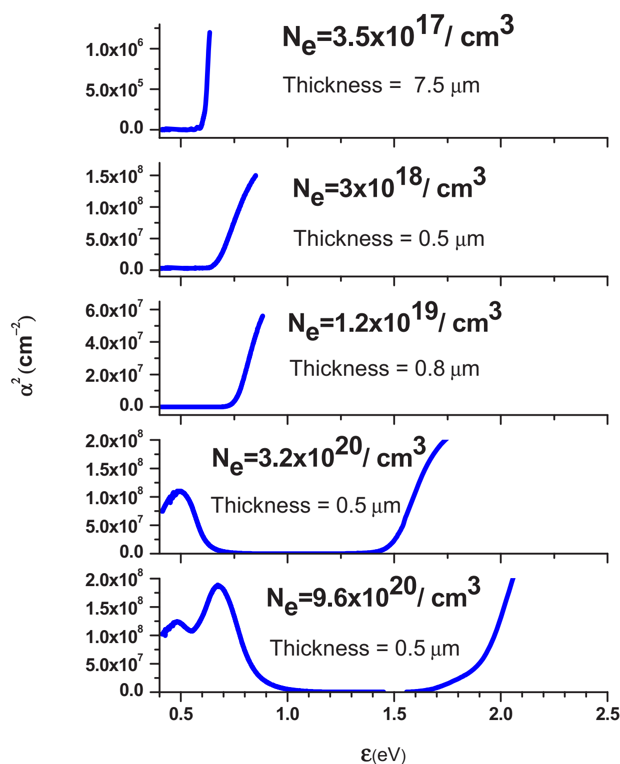

FIG. 1. (Color online) Experimental values of the square of absorption coefficient, α^2 (cm^{-2}), versus photon energy (eV) for InN films with different carrier densities. The values of carrier density and film thickness for each film are written in its panel.

These measurements show that all the films are *n* type and their carrier concentration varies from 10^{17} to 10^{21} cm^{-3}. For all our samples, the Mott critical density $N_c \approx (0.25/a_B^*)^3$ (a_B^* is the effective Bohr radius) is much smaller than the carrier density. For example, for our lowest-density sample with $N_e = 3.5 \times 10^{17}/\text{cm}^3$, the value of N_c is $\sim 5 \times 10^{16}/\text{cm}^3$. So, the carriers in these films are degenerate moving freely in the conduction band.

X-ray diffraction measurements show that the films are of polycrystalline wurtzite nature when grown at 325 °C, whereas completely *c*-axis-textured growth occurs at 475 °C, consistent with Raman scattering studies. These high carrier concentrations may result from the presence of either nitrogen vacancies and/or the other species of impurities and defects typically encountered in InN films.[40,41] Recently, Mahboob *et al.*[20] observed that positively charged donor-type surface states can contribute to an electron accumulation on a clean InN surface. In this paper, we have neglected this electron accumulation phenomenon observed on the clean InN surface[20] and assumed a uniform density profile for the electron distribution whose density value measured by the Hall measurement represents the bulk value.

Figure 1 shows, for different values of N_e, the square of the spectral absorption coefficient α^2. The coefficient α is determined from the measured transmission and reflectance data after correcting for multiple reflections. The reflectance measurements were done with unpolished backside of the sapphire substrate. Sometimes for the reflectance, a constant value independent of energy is considered while estimating α from the transmittance measurements. We used the energy-dependent reflectance for the determination of α. For the transmittance measurements, we polished the backside of the sapphire substrate and then measured the transmittance spectra. Scattering from the backside of the sapphire substrate, although small, affects the values of α for all energies including small energies. For all the samples, film thicknesses were measured from the interference pattern of the reflectance and the transmittance spectra. As the value of N_e increases, the absorption edge widens. For films grown by MBE techniques, the absorption edge varies from 0.61 to 0.70 eV. By contrast, in the PSMBE samples, it ranges from 1.50 to 1.90 eV. The variation of optical-absorption edge in PSMBE samples is attributed to the high electron degeneracy and presence of defect effects. We now analyze the physical mechanism for this widening by taking the electron-electron, electron impurity, and electron-LO phonon in the electronic excitation process.

III. THEORY AND DISCUSSION OF EXPERIMENTAL RESULTS

Figure 1 shows a transparent region at intermediate energy, followed by an absorption edge where a sharp rise in the optical absorption occurs. At this point, a direct band gap transition by the excitation of electron-hole pairs dominates the absorption process. From the experimental absorption spectrum of α^2, the value of the band gap is estimated in the first instance from the intersection on the energy axis of the linear portion of α^2. This estimate is valid only for low carrier densities when the conduction band is almost empty and the electronic transitions are from the valence bands onto the bottom states of the conduction band.

The situation is quite different at higher carrier densities, however. The Fermi energy, which lies in the conduction band, now dictates the occupation of the energy states. Therefore, the energy cost for promoting a valence electron to the conduction band involves, in addition to the band gap energy, the Fermi energy, and, additionally, the so-called self-energies gained from the electron-electron, electron-impurity, and electron-LO-phonon interactions. Simultaneously, the hole created in the valence band will also gain energy by interacting both with defects and carriers (electrons and other holes). All these energy terms have to be supplied by the incident photon when exciting the electron into the conduction band. For this reason, the absorption edge inevitably shifts toward the higher-energy side as the carrier density increases.

In order to extract the intrinsic band gap value for the degenerate and low-density samples, the effects of interaction and degeneracy energies must be taken into consideration in the absorption spectra. We fitted the experimental values of α by evaluating the quantum-mechanical transition rate.[42] In the transition probability model, we assume that all the initial valence band states are filled. In the wave vector selection rules, a small wave vector of the excitation photon is neglected while initial and final states of the electron are assumed to have the same wave vector. In the energy-dependent effective matrix elements for the transition prob-

ability, we considered the effects of the electron-electron, electron-hole, electron-charged impurities, and electron-LO-phonon interactions. Like the band gap value of InN films, the values of electron and hole effective masses are not very well known yet. Their values are normally extracted from electrical or optical measurements by substituting into the expression, for example, the plasma-resonance position, the values of parameters such as carrier density and dielectric constant which are not known very precisely. The values of high-frequency dielectric constant determined with different methods have resulted in different values ($0.11m_0$, $0.12m_0$, $0.14m_0$, and $0.24m_0$, here m_0 is the free-electron mass) of the electron effective mass perpendicular to the c axis. Kasic *et al.*[23] used infrared spectroscopy ellipsometry and Hall-effect measurements to determine a precise value of the electron effective mass which also agreed with the theoretical prediction.[43] However, the widely accepted value[16,43] at the bottom of conduction band at Γ point is considered, $0.07m_0$. Although there is a small anisotropy in the electron effective mass, we have neglected it and considered isotropic values. For the electron dispersions, we have used density-dependent electron effective mass.[16,23] The effective masses for the light and heavy holes are calculated[43–45] within the empirical pseudopotential method approach using ionic model potential parameters and their calculated values[44,45] agree with one another. In our calculations, for the hole dispersion, a density-independent value[44,46] for the hole effective mass is considered. One of the effects of nonparabolic[25,31,32] bands is that the carriers' effective mass becomes dependent on band-edge energy or carrier density. We have taken parabolic bands for the electron and hole dispersions; the nonparabolicity effects, to a large extent, are taken into consideration through the effective-mass values of electrons and holes. The quantum-mechanical transition rate is given by

$$\alpha(\hbar\omega) = \alpha_0 \int_{x_0}^{\infty} dx[x + \hbar\omega - \Delta(k_F)]^{1/2} \frac{\Lambda}{x^2 + \Lambda^2} \times \left[1 - \frac{1}{1 + \exp(\{[x + \hbar\omega - \Delta(k_F)]/m_r - \mu\}/k_B T)} \right]. \quad (1)$$

Here, $\hbar\omega$ is the incident photon energy, $x_0 = \varepsilon_F m_r + \Delta(k_F) - \hbar\omega$, $x = \varepsilon_k m_r + \Delta(k_F) - \hbar\omega$, and α_0 is a constant. $\varepsilon_k = \hbar^2 k^2 / 2m_e^*$ is the free electron dispersion, $m_r = 1 + m_e^*/m_h^*$, Fermi wave vector $k_F = (3\pi^2 N_e)^{1/3}$, Fermi energy $\varepsilon_F = \hbar^2 k_F^2 / 2m_e^*$, and μ is the chemical potential. m_e^* and m_h^* are the effective masses for electron and hole, respectively. The slower initial rise of the experimental $\alpha(\hbar\omega)^2$ near the absorption edge for higher-density films is due to the collisional broadening of the initial and final states taken into account via the broadening parameter Λ. Its value for each spectrum is selected by fitting the experimental curve near the edge. For high densities, we find that the absorption spectra are well reproduced with $\Lambda \sim 0.1$ eV. For low densities, we find that $\Lambda \sim 0.04$ eV. When Λ goes to zero, one recovers the usual energy conservation term of the golden-rule transition expression. From the Fermi distribution function in Eq. (1), it is clear that $\alpha(\hbar\omega)$ begins to increase abruptly when incident energy $\hbar\omega$ is close to the absorption edge energy E_{edge}, i.e., when $\hbar\omega = E_{edge} = \Delta(k_F) + \mu m_r$. Here, $\Delta(k_F)$ measures the minimum energy between the valence and conduction bands and is directly related to the electron and hole interaction energies. With the inclusion of these interactions, the bare-band dispersions become[36,47]

$$E_c(k,\omega) = E_c^0(k) + \hbar\Sigma_c(k,\omega) \quad (2)$$

and

$$E_v(k,\omega) = E_v^0(k) + \hbar\Sigma_v(k,\omega), \quad (3)$$

for conduction and valence bands, respectively. Here, $E_c^0(k) = E_g + \hbar^2 k^2 / 2m_e^*$ is the dispersion for the electrons and $E_v^0(k) = -\hbar^2 k^2 / 2m_h^*$ for the holes. E_g is the band gap energy of undoped films. These energies define the Moss-Burstein shifted band gap according to $E_g^0 = E_c^0(k_F) - E_v^0(k_F) = E_g + m_r \varepsilon_F$. Having introduced these energies, we can define the frequency independent $\Delta(k_F) = E_g + \hbar\Sigma_c(k_F) - \hbar\Sigma_v(k_F)$. We have neglected hole-electron contributions to the self-energy. E_g for each film can be determined from the experimentally observed absorption edge energy using equations $E_{edge} = \Delta(k_F) + \mu m_r$ and $\Delta(k_F) = E_g + \hbar\Sigma_c(k_F) - \hbar\Sigma_v(k_F)$ according to

$$E_g = E_{edge} - \hbar\Sigma_c(k_F) + \hbar\Sigma_v(k_F) - \mu m_r. \quad (4)$$

We calculate electron-electron self-energy according to the standard GW approximation,[48–50] taking the leading-order expansion of the dynamic screened potential as

$$\hbar\Sigma_c^{ee}(k, i\omega_l) = \frac{1}{(2\pi)^3} \int dq T \sum_{\omega_n} V_{sc}(q, i\omega_n) \frac{1}{i\omega_l + i\omega_n - \varepsilon_{q-k}}. \quad (5)$$

Here, $i\omega_l = i(2l+1)\pi k_B T$ and $i\omega_n = i2n\pi k_B T$ are the fermion and/or boson odd and/or even Matsubara frequencies (l, m integers). The dynamic screened potential $V_{sc}(q, i\omega_n) = V(q)/\varepsilon(q, i\omega_n)$ is given in terms of dynamical dielectric function $\varepsilon(k, i\omega_n) = 1 + V(q)\chi(q, i\omega_n)$. Here, $V(q) = 4\pi e^2 / \varepsilon_0 q^2$ is the Fourier transform of the Coulomb potential and ε_0 is the dielectric constant. Anisotropy of the dielectric function for wurtzite InN films is very small. Persson *et al.*[30] calculated dielectric constant using a full-potential linearized augmented plane-wave method. Using the exchange-correlation potential of Engel and Vosko, they found that the value of dielectric constant is 6.7, while with Perdew and Wang exchange-correlation potential, the value becomes 9.5. Furthmuller *et al.*[21] estimated the dielectric constant using ab initio calculations and found it to be ~7.2, which agrees with the calculated value by Christensen and Gorczyca.[51] Using first-principles orthogonal linear combination of atomic-orbital method in the local density approximation, Xu and Ching[52] found a value equal to 7.6. There are not much experimental data on the values of dielectric constant. An old measurement gave $\varepsilon_0 = 8.2$, while recent experiment by Kasic *et al.*[23] gave a smaller value of 6.7. The static screening function $\varepsilon(k, \mu) = 1 + V(q)\chi(q, \mu)$ is calculated with an appropriate value of μ determined for each sample. $\chi(q, i\omega_n)$ is the temperature-dependent electron polarizability and within the

random-phase approximation,[53] it can be written as

$$\chi(q,i\omega) = \frac{-2}{(2\pi)^2}\frac{m_e^*}{\hbar^2 q}\int_0^\infty dkkn_F(\varepsilon_k) \times\left[\ln\left|\frac{i\omega-\hbar^2q^2/2m_e^*-\hbar^2qk/2m_e^*}{i\omega-\hbar^2q^2/2m_e^*+\hbar^2qk/2m_e^*}\right| + \ln\left|\frac{i\omega+\hbar^2q^2/2m_e^*+\hbar^2qk/2m_e^*}{i\omega+\hbar^2q^2/2m_e^*-\hbar^2qk/2m_e^*}\right|\right]. \quad (6)$$

Here, $n_F(x)=1/[e^{(x-\mu)/k_BT}+1]$ is the Fermi distribution function. The quasiparticle self-energy is now obtained by evaluating the real part of the retarded self-energy $\hbar\Sigma_c^{ee}(k,i\omega_l \to \omega+i0^+)=\hbar\Sigma_c^{ee}(k,\omega)$. For the numerical evaluation of the self-energy, we use the frequency integration method.[54] The retarded self-energy becomes

$$\mathrm{Re}\,\hbar\Sigma_c^{ee}(k,\omega) = -\frac{1}{(2\pi)^3}\int dqV(q)n_F(\varepsilon_{q-k}) - \frac{2}{(2\pi)^4}\int dq \times\int d\omega' V(q)\mathrm{Im}\frac{1}{\varepsilon(q,\omega')}\frac{n_B(\omega')+n_F(\varepsilon_{q-k})}{\omega'+\omega-\varepsilon_{q-k}}, \quad (7)$$

where $n_B(x)=1/(e^{x/k_BT}-1)$ is the Bose distribution function. For the valence band, the corresponding equation for the self-energy can be written[36] as

$$\hbar\Sigma_v^{ee}(k,i\omega_l) = \frac{1}{(2\pi)^3}\int dqT\sum_{\omega_n}[V_{sc}(q,i\omega_n)-V(q)] \times\frac{1}{i\omega_l+i\omega_n-\varepsilon_{q-k}}. \quad (8)$$

In films having a large number of defects, the band edges are not very well defined as is clearly observed in the absorption spectra of the films. At higher impurity concentrations, the impurity band may merge with the conduction band and reduce the size of the band gap. The availability of additional density of states, near the band gap produced by the electron-impurity and electron-LO-phonon interactions, will change the value of chemical potential for the same (fixed) value of carrier density according to the equation

$$N_e = \int_{-\infty}^{\infty}\frac{\rho(\varepsilon)}{\exp[(\varepsilon-\mu)/k_BT]+1}d\varepsilon. \quad (9)$$

For strongly degenerate films, the chemical potential is the largest energy parameter affecting the absorption spectrum [Eq. (1)] through the Fermi-Dirac distribution function. We determine $\rho(\varepsilon)$ by incorporating the electron-impurity and electron-LO-phonon interaction energies through the single-electron Green's function[55] $G(q,\varepsilon)$, using equation

$$\rho(\varepsilon) = \frac{2}{\pi}\sum_q \mathrm{Im}\,G(q,\varepsilon) = \frac{2}{\pi}\sum_q \mathrm{Im}\,\frac{1}{\varepsilon-\varepsilon_q-\Sigma_c^{eimpL}(q,\varepsilon)}. \quad (10)$$

Here, the self-energy, $\Sigma_c^{eimpLO}(q,\varepsilon)=\Sigma_c^{eimp}(q,i\omega_l)+\Sigma_c^{eLO}(q,i\omega_l)$, represents contributions from ionized impurities and LO phonons. For the electron-impurity component, $\Sigma_c^{eimp}(q,i\omega_l)$, we assume that the impurities are rigidly fixed, allowing no exchange of energy and momentum (elastic scattering only) and are homogeneously distributed. Because the impurities are strictly passive, they will be screened purely by the static screening function $\varepsilon(k,\mu)$ of the electrons. The self-energy due to electron-impurity interaction can be written[55,56] as

$$\Sigma_c^{eimp}(k,i\omega_l) = N_i\sum_q \frac{V(q)^2}{\varepsilon(q,\mu)^2}\frac{1}{i\omega_l-\varepsilon_{q-k}}. \quad (11)$$

Due to the strongly polar nature of the crystal structures of InN films, electrons also gain energy from interacting with the LO phonons. The corresponding self-energy,[57] $\Sigma_c^{eLO}(q,i\omega_l)$, is given as

$$\Sigma_c^{eLO}(k,i\omega_l) = \frac{1}{(2\pi)^3}\int dq\frac{W(q)^2}{\varepsilon(q,\mu)^2}\left[\frac{1+n_B(\omega_{LO})-n_F(\varepsilon_{q-k})}{i\omega_l-\varepsilon_{q-k}-\omega_{LO}} + \frac{n_B(\omega_{LO})+n_F(\varepsilon_{q-k})}{i\omega_l-\varepsilon_{q-k}+\omega_{LO}}\right]. \quad (12)$$

Here, the squared average of the electron-LO-phonon interaction matrix elements is $W(k)^2=[2\pi e^2\hbar\omega_{LO}(1/\varepsilon_\infty-1/\varepsilon_0)2\pi e^2/k^2]^{1/2}$. For the LO-phonon energy,[58] ω_{LO}, we used $\omega_{LO}=590\ \mathrm{cm}^{-1}$ and for the ε_∞, we took 6.7. If we neglect the small value of the LO-phonon energy compared to the electron Fermi energy, the above equation reduces to

$$\Sigma_c^{eLO}(k,i\omega_l) = \frac{2}{(2\pi)^3}\int dq\frac{W(q)^2}{\varepsilon(q,\mu)^2}[n_B(\omega_{LO})+1/2]\frac{1}{i\omega_l-\varepsilon_{q-k}}. \quad (13)$$

This expression can now be combined with the electron-impurity self-energy expression [Eq. (11)] to get the total self-energy, $\Sigma_c^{eimpLO}(q,\varepsilon)$, at ε_F:

$$\Sigma_c^{eimpLO}(k,\varepsilon_F) = \sum_q\frac{1}{\varepsilon(q,\mu)^2}\{N_iV(q)^2+2W(q)^2 \times[n_B(\omega_{LO})+1/2]\}\frac{1}{\varepsilon_F-\varepsilon_{q-k}}. \quad (14)$$

In the above equation, the temperature-dependent static screening function is calculated by setting $\omega=0$ in Eq. (6). The imaginary part of the self-energy defines the electron relaxation time and we calculate its inverse, the relaxation rate (or quasiparticle linewidth), using the "mass-shell" approximation, i.e., $\Sigma_c^{eimpLO}(k=k_F,\varepsilon=\varepsilon_F)=i\Gamma$. The above equation is generalized to self-consistently calculate the self-energy, and thus the electron relaxation time, by adding the self-energy term $\Sigma_c^{eimpLO}(k,\varepsilon_k)$ to its energy denominator.

Neglecting the real part of the self-energy compared to other energy terms one gets from Eq. (14), after substituting for the expressions of $V(q)$ and $W(q)$, a nonlinear equation for the net electron relaxation rate Γ as a function of N_i. It is given by

$$\Gamma = \sum_k \frac{1}{\varepsilon(k,\mu)^2}\left\{ N_i \frac{4\pi e^2}{\varepsilon_\infty k^2} + \frac{2}{k}\left[2\pi e^2 \hbar \omega_{LO} \times \left(\frac{1}{\varepsilon_\infty} - \frac{1}{\varepsilon_O} \right) \right]^{1/2} [n_B(\omega_{LO}) + 1/2] \right\} \frac{\Gamma}{(\varepsilon_F - \varepsilon_k)^2 + \Gamma^2}. \quad (15)$$

In addition to screened-impurity scattering, other types of defects present in InN films will also contribute to the scattering rates and thus to the self-energy. The effects of these defects on Γ and other properties can be incorporated, to an extent, by adjusting the values of N_i in the above equation. Using the self-consistently determined Γ from Eq. (15), we calculate $\rho(\varepsilon)$ from Eq. (10) within the mass-shell approximation. In the limit $\Gamma \to 0$, one recovers the usual $\sqrt{\varepsilon}$ type of DOS. However, for finite values of Γ, there is a spilling of the DOS into the band gap region. This new distribution of DOS modifies the value of chemical potential for a given value of N_i. For an experimentally measured value of N_e, we can determine the corresponding values of μ as a function of N_i.

Since both Γ and μ are interdependent quantities, it is important to self-consistently solve them using Eqs. (9), (10), and (15). We solved them using the following procedure.

(1) First, for a given N_i, we solve for Γ using Eq. (15) starting with an initial guess for $\mu = \varepsilon_F$,

(2) we then use this Γ to calculate $\rho(\varepsilon)$ and then determine a new value of μ from Eq. (9),

(3) we use this new value of μ in Eq. (15) through $\varepsilon(k,\mu)$, and finally,

(4) repeat the whole iteration process until we get self-consistent solutions for both μ and Γ.

The value of μ affects the screening function and thus the scattering rates of electrons and holes which in turn affect the self-energies. Most importantly, μ shifts the absorption edge. So, in Eq. (1) for the optical-absorption spectra, it is important that an appropriate value of μ is used in the Fermi-Dirac distribution function that also takes into account the temperature effect.

As discussed above, the values of dielectric constant for InN films are found to vary within a certain range. In the estimation of the band gap values, we considered two values, 8 and 10, for ε_0 to screen the electron interaction potentials. For each carrier density, we self-consistently calculated μ as a function of impurity concentration $C_i = N_i/N_e$ for the two values of ε_0, and for each value of ε_0, we took two diverse values of m_e^* generally used[16,23] for that value of electron density. Figures 2(a), 3(a), 4(a), 5(a), and 6(a) show the self-consistently calculated μ as a function of C_i and two panels in these figures represent μ calculated for two different values of electron effective mass. For a given value of ε_0, electron degeneracy increases when the value of m_e^* decreases and this effect, as expected, is reflected through increase in the values of μ. On the other hand, when ε_0 increases for a fixed value of m_e^*, the electron impurities and electron-LO-phonon self-energies decrease due to the stronger screening and this increases the values of μ, as seen in Figs. 2(a), 3(a), 4(a), 5(a), and 6(a). The values of μ steadily decrease with

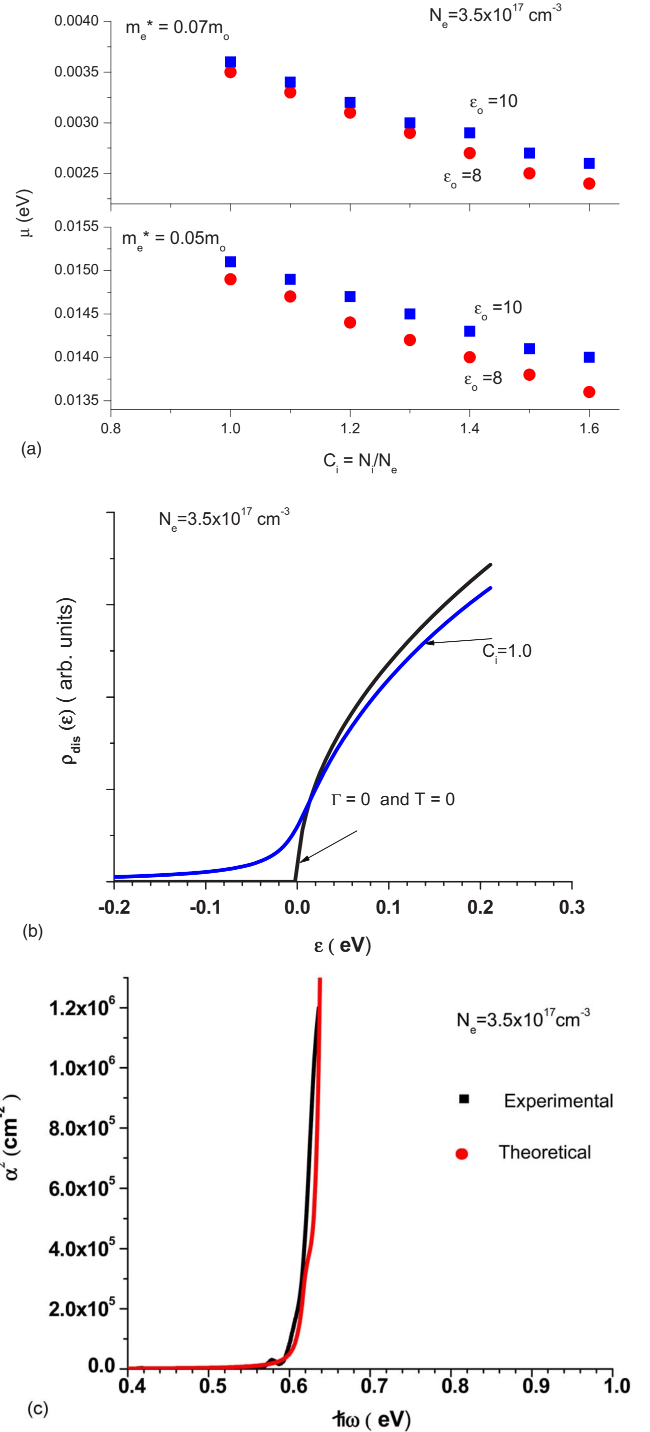

FIG. 2. (Color online) (a) Self-consistently determined μ (eV) for two values of m_e^* as a function of C_i for the film with carrier density $N_e = 3.5 \times 10^{17}$ cm^{-3}. Upper and lower panels show μ (eV) calculated using $m_e^* = 0.07m_0$ and $0.05m_0$, respectively. Each panel shows μ (eV) for the two values, 8 (solid red circles) and 10 (solid blue squares), of ε_0. The values of ε_0 are marked against their plots. (b) DOS as a function of energy (eV) for two values of impurity concentrations. Here, DOS are calculated for $m_e^* = 0.05m_0$ and $\varepsilon_0 = 10$. (c) The experimentally (solid-square curve) measured and theoretically calculated (solid-circle curve) α^2 (cm^{-2}) for $C_i = 1.1$ as a function of energy (eV). Theoretical data are only calculated for energies near the absorption edge.

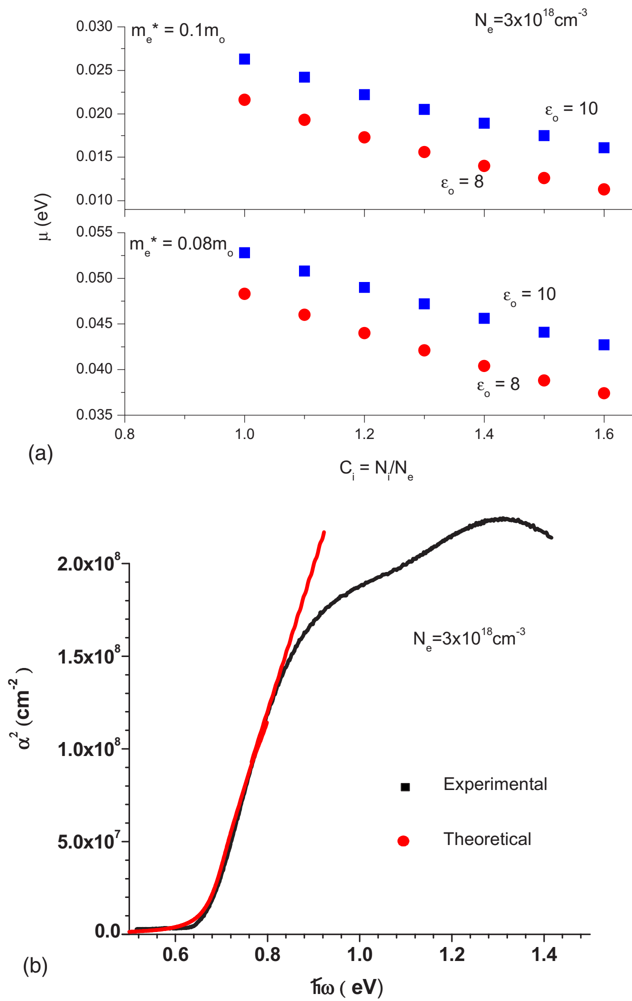

FIG. 3. (Color online) (a) Self-consistently determined μ (eV) for two values of m_e^* as a function of C_i for the film with carrier density $N_e=3.0\times 10^{18}$ cm^{-3}. Upper and lower panels show μ (eV) calculated using $m_e^*=0.10m_0$ and $0.08m_0$, respectively. Each panel shows μ (eV) for the two values, 8 (solid red circles) and 10 (solid blue squares), of ε_0. The values of ε_0 are marked against their plots. (b) The experimentally (solid-square curve) measured and theoretically calculated (solid-circle curve) α^2 (cm^{-2}) for $C_i=1.1$ as a function of energy (eV). Theoretical data are only calculated for energies near the absorption edge.

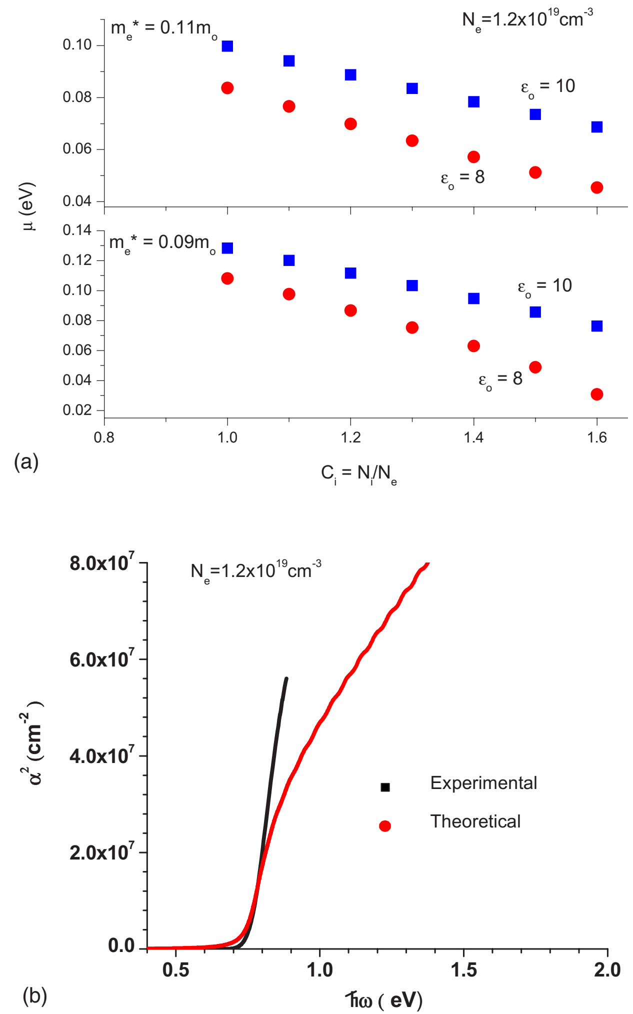

FIG. 4. (Color online) (a) Self-consistently determined μ (eV) for two values of m_e^* as a function of C_i for the film with carrier density $N_e=1.2\times 10^{20}$ cm^{-3}. Upper and lower panels show μ (eV) calculated using $m_e^*=0.11m_0$ and $0.09m_0$, respectively. Each panel shows μ (eV) for the two values, 8 (solid red circles) and 10 (solid blue squares), of ε_0. The values of ε_0 are marked against their plots. (b) The experimentally (solid-square curve) measured and theoretically calculated (solid-circle curve) α^2 (cm^{-2}) for $C_i=1.1$ as a function of energy (eV). Theoretical data are only calculated for energies near the absorption edge.

increasing values of C_i showing a significant departure from the Fermi energy value. Normally, the chemical potential is replaced with Fermi energy in the discussion of optical and electrical transport properties, and this could lead to either an under- or overestimation of the physical parameters derived from these properties.

The physical significance of μ in the optical-absorption spectra is that it provides a rough estimate for the shift in the absorption edge beyond the conduction-band minimum coming from the self-energy gain due to defects and phonons at finite temperature. Figures 2(a), 3(a), 4(a), 5(a), and 6(a) show that the shift in the absorption edge for a film with a larger number of defects is small compared to a film with a smaller number of defects. The values of μ also increase with carrier density due to the stronger degeneracy effect and this is consistent with the experimentally observed shifts in absorption edge which widens as the carrier density of the samples increases. In an n-type semiconductor, the crystal must contain resonance states or shallow donors which can be thermally excited at room temperature to generate free carriers. The origins of the high carrier concentrations are not very well understood yet for InN thin-film materials. However, a possible origin of donors has been associated with the excess nitrogen which sits on the antisite defects; this antisite is a double donor with shallow first-ionization energy.

For GaN and AlN, the carrier density values are much smaller.[59] In GaN, a nitrogen vacancy introduces a shallow donor level and may be responsible for the n-type conductivity in this material. Owing to the wide band gap of GaN, the self-compensation effects[60] strongly reduce both the

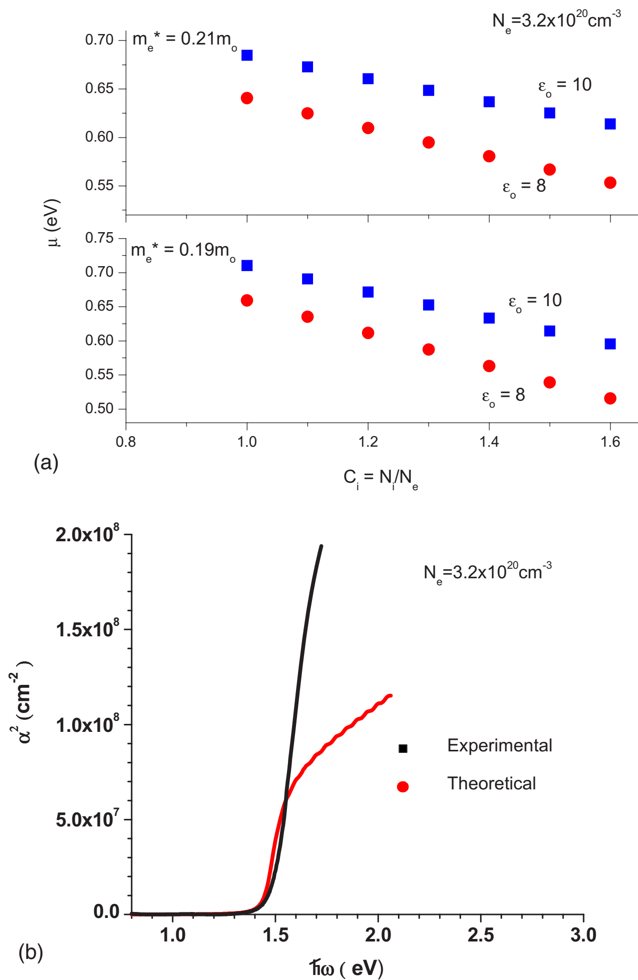

FIG. 5. (Color online) (a) Self-consistently determined μ (eV) for two values of m_e^* as a function of C_i for the film with carrier density $N_e = 3.2 \times 10^{20}$ cm^{-3}. Upper and lower panels show μ (eV) calculated using $m_e^* = 0.21 m_0$ and $0.19 m_0$, respectively. Each panel shows μ (eV) for the two values, 8 (solid red circles) and 10 (solid blue squares), of ε_0. The values of ε_0 are marked against their plots. (b) The experimentally (solid-square curve) measured and theoretically calculated (solid-circle curve) α^2 (cm^{-2}) for $C_i = 1.1$ as a function of energy (eV). Theoretical data are only calculated for energies near the absorption edge.

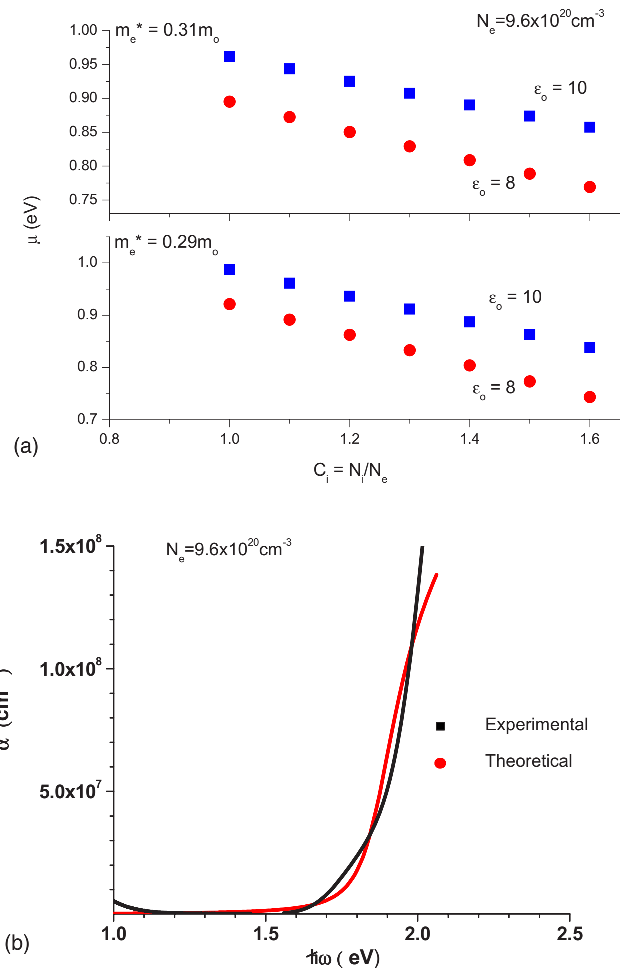

FIG. 6. (Color online) (a) Self-consistently determined μ (eV) for two values of m_e^* as a function of C_i for the film with carrier density $N_e = 9.6 \times 10^{20}$ cm^{-3}. Upper and lower panels show μ (eV) calculated using $m_e^* = 0.31 m_0$ and $0.29 m_0$, respectively. Each panel shows μ (eV) for the two values, 8 (solid red circles) and 10 (solid blue squares), of ε_0. The values of ε_0 are marked against their plots. (b) The experimentally (solid-square curve) measured and theoretically calculated (solid-circle curve) α^2 (cm^{-2}) for $C_i = 1.1$ as a function of energy (eV). Theoretical data are only calculated for energies near the absorption edge.

n-type and *p*-type doping efficiency due to the respective formation of Ga vacancies and interstitial Ga. Because of the smaller values of carrier density for GaN and AlN, one expects smaller shifts in the values of μ relative to the Fermi energies or, in other words, smaller shifts in the absorption edge relative to the conduction-band minima. Determination of these energy parameters (μ, Fermi energy, and absorption edge) is important for the estimation of the band gap value, which is smallest for InN compared to GaN and AlN. Although the value of the dielectric constant for InN film is larger than GaN and AlN, the generally observed values of carrier density are much larger for InN leading to larger electron-impurity interaction effects in InN compared to other nitrides. The second component is the contribution from the electron-LO-phonon interaction. The values of scaled electron-LO-phonon coupling constant[59] $\alpha/(2\pi e^2) = \hbar\omega_{LO}(1/\varepsilon_\infty - 1/\varepsilon_0)$ are 10.7, 7.2, and 4.8 meV for AlN, GaN, and InN, respectively.

In addition to the presence of defects, the temperature also affects the value of μ. The chemical potential decreases with increasing temperature and this effect becomes more pronounced if the Fermi energy is smaller than the thermal energy. Basically, the temperature affects the screening function through the distribution functions of the electrons; it also affects the distribution function for the LO phonons. Wu *et al.*[16,61] studied the influence of temperature on the absorption edge and found that it decreases with increasing values of temperature. For lower-density samples, they found that the shift in the absorption edge with temperature is larger compared to higher-density samples. A simple correction to the absorption edge due to the Moss-Burstein shift, which depends on temperature-independent parameters—the effective

masses of electron and holes and the electron density—cannot explain this experimental observation.

Figure 2(b) shows $\rho(\varepsilon)$ at carrier density $N_e=3.5\times10^{17}$ cm^{-3} for two cases: one for $C_i=1$ and other when $\Gamma=0$, means electron-defect and electron-LO-phonon interactions are absent. Electron interaction with defects changes the distribution of the DOS with respect to the energy values and this behavior is observed, in general, for all values of carrier density. Electron-defect interaction suppresses the DOS values for those states which are high in energy within the conduction band, creating a band tailing effect near the conduction-band edge region as expected for disordered semiconductor materials. Similar behavior for the DOS has also been proposed using the argument of potential fluctuations[31] arising from the Coulomb potentials of charged impurities randomly distributed in the system. Here, the root-mean-square potential-energy fluctuations, related to the band tailing, are calculated from the screening length parameter.

Although InN, GaN, and AlN are members of the same group-III-nitride family, their typical carrier density, electron effective mass, and other physical parameters are very diverse.[60] This could result in very different values of self-energies for InN, GaN, and AlN films. One of the characteristics of the electron effective mass of InN film is its strong dependence on the carrier density in contrast to GaN and AlN films. Further, its value increases with the increasing value of carrier density.[16,23] The electron effective mass for InN is also smaller than that of GaN and AlN semiconductors. A smaller effective mass increases the degeneracy energy and also affects the screening function. The values of carrier density for InN films are also significantly higher from GaN and AlN films. The typical electron concentrations in InN are in the $10^{19}-10^{20}$ cm^{-3} range, which are higher than generally observed values in GaN and even much higher than unintentionally doped AlN thin films. So, the self-energy contributions due to electron-electron and electron-defect interactions are expected to be larger for InN films than AlN and GaN films.

AlN films are highly resistive generally in the $10^{11}-10^{13}$ Ω cm range, indicating the presence of sufficiently deep native defects. Experimental investigations[62–64] for AlN have observed states lying roughly 170, 500, and 800–1000 meV below the conduction-band edge due to donor triplet of the nitrogen vacancy, while other works[64,65] have detected deeper levels lying between 1.4 and 1.85 eV, speculated to be due to the N antisite defect. These types of states have negligible contribution to electron-defect self-energy due to small concentrations of electrons and charged ions at room temperature.

Persson *et al.*[59] have calculated the doping-induced energy shift for GaN and AlN semiconductors by calculating electron-electron, electron-exchange, electron-impurity, and electron-LO-phonon interactions using a zero-temperature formalism. The screening function used by Persson *et al.*[59] is expressed in terms of static and high-frequency dielectric constants. However, while their screening function includes scattering effects from the long-wavelength LO phonons, it is independent of temperature, electron density, and wave vector. These parameters can strongly affect the screening and thus the self-energy values. The dielectric constant and electron effective-mass values are roughly the same for the AlN and GaN in the wurtzite structure, so one expects similar values for the self-energies in both the nitrides. However, for the InN films, the values of the physical parameters—effective masses of carriers, dielectric constant, and carrier density—are different and this will result in different values of self-energies.

Polaron effect in semiconductors can also lead to the shrinkage of the band gap if the energy gained is significant. In InN films, the dominant electron-phonon interaction comes from the electron interaction with LO phonons. In the calculation of the chemical potential which affects the optical-absorption edge, we have considered this interaction effect using temperature-dependent screening function.

For direct band gap semiconductors, the optical-absorption edge contains the band-filling energy contribution due to the Moss-Burstein shift which, here in our calculations, is incorporated into the chemical potential. Within the Hartree-Fock approximation, the analytical expression for the self-energy $\hbar\Sigma_c^{HF}(0)$ can be easily obtained.[36] One gets a simple temperature-independent expression $\hbar\Sigma_c^{HF}(0)=-2e^2(3\pi N_e)^{1/3}/\varepsilon_0\pi$ which does not contain electron-defect interaction and correlation effects. In the more general expressions, Eqs. (7) and (8), the effects from electron-defect scattering, electron-LO-phonon scattering, electron correlation, and temperature are included. The energy shift in the valence band due to the exchange contribution is ignored, assuming that it is fully occupied. The self-energies of an electron depend strongly on the values of carrier density and impurity density. Other important physical parameters which influence the self-energies are the dielectric constant ε_0 which reduces the Coulomb energy, the electron-LO-phonon coupling constant, and electron and hole effective masses.

In the self-energy calculations of a film of a given N_e, we used the corresponding self-consistently calculated μ in the screening function of the self-energies. Knowing both the self-energies and μ, we extract the values of band gap energy $E_g=E_{edge}-\hbar\Sigma_c(k_F)+\hbar\Sigma_v(k_F)-\mu m_r$ from the experimental absorption edge value E_{edge} for each film as a function of C_i. The variations in the values of E_g for each film are discussed with parameters m_e^* and ε_0 which affect directly μ and the electron interaction energies, respectively. Indirectly, μ is also affected by ε_0 through the relaxation rate Γ. Similarly, the self-energies, $\hbar\Sigma_c(k_F)$ and $\hbar\Sigma_v(k_F)$, are also affected indirectly by m_e^* through μ. The changes in E_g when ε_0 is varied from 8 to 10 are small compared to the changes due to the variations in the values of m_e^*. In general, the calculated values of E_g increase with increasing defect concentrations due to the decrease in the values of μ. In Table I, we show the results for our calculated values of E_g at $C_i=1.1$. For our lowest-density film, the variations in the calculated values of E_g with respect to both m_e^* and ε_0 are not significant. The values of E_g are slightly larger for $\varepsilon_0=10$ compared to $\varepsilon_0=8$ due to the larger variations in self-energies compared to μ. The values of E_g for the film with a carrier density of 1.2×10^{19}/cm^3 vary from ~0.59 to ~0.63 eV for the chosen values of m_e^* and ε_0. For our highest-density film, the values of E_g vary from ~0.60 to ~0.68 eV, depending on

TABLE I. Calculated E_g (eV) at $C_i=1.1$ for $\mathcal{E}_0=8$ and 10 for two different values of m_e^*. The carrier densities of the films are shown in the first column.

N_e (cm^{-3})	$\mathcal{E}_0$	m_e^*	E_g (eV)
3.5×10^{17}	8.0	$0.5m_0$	0.58
		$0.07m_0$	0.59
	10.0	$0.05m_0$	0.60
		$0.07m_0$	0.60
3.0×10^{18}	8.0	$0.8m_0$	0.60
		$0.10m_0$	0.63
	10.0	$0.08m_0$	0.60
		$0.10m_0$	0.62
1.2×10^{19}	8.0	$0.9m_0$	0.61
		$0.11m_0$	0.63
	10.0	$0.09m_0$	0.59
		$0.11m_0$	0.61
3.2×10^{20}	8.0	$0.19m_0$	0.66
		$0.21m_0$	0.65
	10.0	$0.19m_0$	0.61
		$0.21m_0$	0.60
9.6×10^{20}	8.0	$0.29m_0$	0.68
		$0.31m_0$	0.68
	10.0	$0.29m_0$	0.60
		$0.31m_0$	0.61

the values of m_e^* and ε_0, which is consistent with the other measurements.[2,17] Using the calculated value of E_g and the corresponding value of self-consistently determined μ, we fitted the experimentally determined absorption spectrum for each sample. The results for all the samples are shown in Figs. 2(c), 3(b), 4(b), 5(b), and 6(b).

Some of the polycrystalline films show[66] an almost flat absorption edge even when the carrier density in the films increases by several orders of magnitude. One observes from Eq. (1) that the absorption is exponentially suppressed by the Fermi-Dirac factor for incident photon energies smaller than $E_g+\mu m_r$, assuming that E_g is the dominant energy factor (for InN films) in $\Delta(k_F)$. The chemical potential is one of the important energy factors which control this behavior. As discussed above, its value decreases with increasing levels of defect concentration in the films. In these polycrystalline films, fabricated with different techniques,[66] the level of defects emanating from various sources such as grain boundaries, etc., is not very well known. Nevertheless, irrespective of the nature of the defects, one of its effects is to modify the value of μ. A possible explanation for the flat absorption edge at increasing carrier densities is that the level of defects in these films increases much more rapidly so that the corresponding value of the chemical potential varies far more slowly with carrier density than would be the case in other films where absorption edge grows with carrier density. If this is so, then for a nearly fixed value of E_g, the absorption edge will stay almost constant with increasing N_e, an effect that is actually observed in these polycrystalline films.

IV. CONCLUSION

In this paper, we have presented measurements of the optical-absorption spectra of InN films fabricated with two different techniques: molecular-beam epitaxy and plasma-source molecular-beam epitaxy. These films exhibit a variation in their carrier density over 3 orders of magnitude: from lightly populated to heavily metallic.

The measured absorption edge increases with the electron density. We have theoretically investigated the roles of electron degeneracy, electron-electron, electron-impurity, and electron-LO-phonon interactions on the absorption edge. We developed a self-consistent method to evaluate dielectric function, scattering rates due to electron-defect and electron-LO-phonon interactions, and chemical potential. The contributions to single-particle energy due to scattering from charged impurities and LO phonons are calculated within the mass-shell approximation. Using the GW and random-phase approximations to model the contributions of these mechanisms to the carrier self-energies, we have computed their contributions to the shift in the observed optical-absorption edge.

We have estimated the true size of the underlying band gap for these films by removing the interaction-induced terms and electron degeneracy effect which shift its measured value away from its intrinsic one. The variations in the values of E_g for each film are discussed for two different values of electron effective mass and static dielectric constant. For the lowest-density film, the estimated values of E_g are close ~0.59 eV while for the highest-density film, they vary from ~0.60 to ~0.68 eV depending on the values of m_e^* and ε_0. We have observed that, for the determination of the band gap value, it is important to use an appropriate value of the chemical potential taking into account the temperature, electron-charged impurities, and electron-LO-phonon interactions effects. Neglect of the carrier self-energies in the analysis of optical absorption can lead to overestimation of the band gap value.

ACKNOWLEDGMENTS

This work was supported by NSF-IGERT-DGE Grant No. 9870720 and by the Center for Smart Sensors and Integrated Microsystems at Wayne State University. We thank H. Lu and W. J. Schaff for providing us the low-density InN films.

*jagdish@wayne.edu

[1] S. C. Jain, M. Willander, J. Narayan, and R. Van Overstraeten, J. Appl. Phys. **87**, 965 (2000).

[2] V. Yu. Davydov *et al.*, Phys. Status Solidi B **229**, R1 (2002); J. Wu, W. Walukiewicz, K. M. Yu, J. W. Ager III, E. E. Haller, H. Lu, W. J. Schaff, Y. Saito, and Y. Nanishi, Appl. Phys. Lett. **80**, 3967 (2002).

[3] H. Sakai, T. Koide, H. Suzuki, M. Yamaguchi, S. Yamasaki, M. Koike, H. Amano, and I. Akasaki, Jpn. J. Appl. Phys., Part 2 **34**, L1429 (1995).

[4] K. Osamura, S. Naka, and Y. Murakami, J. Appl. Phys. **46**, 3432 (1975).

[5] T. Inushima, M. Higashiwaki, and T. Matsui, Phys. Rev. B **68**, 235204 (2003).

[6] H. J. Hovel and J. J. Cuomo, Appl. Phys. Lett. **20**, 71 (1972).

[7] T. Inushima, M. Higashiwaki, T. Matsui, T. Takenobu, M. Motokawa, and T. Matsui, Phys. Rev. B **72**, 085210 (2005).

[8] J. S. Thakur, R. Naik, V. M. Naik, D. Haddad, G. W. Auner, H. Lu, and W. J. Schaff, J. Appl. Phys. **99**, 023504 (2006).

[9] K. Osamura, K. Nakajima, and Y. Murakai, Solid State Commun. **11**, 617 (1972).

[10] T. L. Tansley and C. P. Foley, J. Appl. Phys. **59**, 3241 (1986); **60**, 2092 (1986).

[11] K. L. Westra, R. P. Lawson, and M. J. Bret, J. Vac. Sci. Technol. A **6**, 1730 (1988).

[12] K. Ikuta, Y. Inoue, and O. Takai, Thin Solid Films **334**, 49 (1998).

[13] B. E. Foutz, S. K. O'Leary, M. Shur, and L. F. Eastman, J. Appl. Phys. **85**, 7727 (1999).

[14] K. S. A. Butcher, M. Wintrebert-Fouquet, P. P.-T. Chen, H. Timmers, and S. K. Shrestha, Mater. Sci. Semicond. Process. **6**, 351 (2003).

[15] V. Yu. Davydov *et al.*, Phys. Status Solidi B **230**, R4 (2002).

[16] J. Wu, W. Walukiewicz, W. Shan, K. M. Yu, J. W. Ager III, E. E. Haller, H. Lu, and W. J. Schaff, Phys. Rev. B **66**, 201403(R) (2002); H. Lu, W. J. Schaff, H. Hwang, H. Wu, G. Koley, and L. F. Eastman, Appl. Phys. Lett. **79**, 1489 (2001).

[17] T. Matsuoka, H. Okamoto, M. Nakao, H. Harima, and E. Kurimoto, Appl. Phys. Lett. **81**, 1246 (2002); M. Higashiwaki and T. Matsui, J. Cryst. Growth **269**, 162 (2004).

[18] T. V. Shubina *et al.*, Phys. Rev. Lett. **92**, 117407 (2004).

[19] O. Ambacher, J. Phys. D **31**, 2653 (1998).

[20] I. Mahboob, T. D. Veal, C. F. McConville, H. Lu, and W. J. Schaff, Phys. Rev. Lett. **92**, 036804 (2004); I. Mahboob, T. D. Veal, L. F. J. Piper, C. F. McConville, H. Lu, W. J. Schaff, J. Furthmuller, and F. Bechstedt, Phys. Rev. B **69**, 201307(R) (2004).

[21] J. Furthmüller, P. H. Hahn, F. Fuchs, and F. Bechstedt, Phys. Rev. B **72**, 205106 (2005).

[22] P. Perlin, J. Camassel, W. Knap, T. Taliercio, J. C. Chervin, T. Suski, I. Grzegory, and S. Porowski, Appl. Phys. Lett. **67**, 2524 (1995).

[23] A. Kasic, M. Schubert, Y. Saito, Y. Nanishi, and G. Wagner, Phys. Rev. B **65**, 115206 (2002).

[24] J. S. Thakur, D. Haddad, V. M. Naik, R. Naik, G. W. Auner, H. Lu, and W. J. Schaff, Phys. Rev. B **71**, 115203 (2005).

[25] S.-H. Wei, X. Nie, I. G. Batyrev, and S. B. Zhang, Phys. Rev. B **67**, 165209 (2003); **68**, 199901(E) (2003).

[26] D. C. Look, H. Lu, W. J. Schaff, J. Jasinski, and Z. Liliental-Weber, Appl. Phys. Lett. **80**, 258 (2002).

[27] T. Araki, S. Ueta, K. Mizuo, T. Yamaguchi, Y. Saito, and Y. Nanishi, Phys. Status Solidi C **0**, 2798 (2003).

[28] F. Bechstedt, J. Furthmüller, O. Ambacher, and R. Goldhahn, Phys. Rev. Lett. **93**, 269701 (2004).

[29] T. V. Shubina *et al.*, Phys. Rev. Lett. **93**, 269702 (2004); T. V. Shubina *et al. ibid.* **95**, 209901(E) (2005).

[30] C. Persson, R. Ahuja, A. F. da Silva, and B. Johansson, J. Phys.: Condens. Matter **13**, 8945 (2001).

[31] P. Carrier and S. H. Wei, J. Appl. Phys. **97**, 033707 (2005).

[32] F. Bechstedt, J. Furthmüller, M. Ferhat, L. K. Teles, L. M. R. Scolfaro, J. R. Leite, V. Yu. Davidov, O. Ambacher, and R. Goldhahn, Phys. Status Solidi A **195**, 628 (2003).

[33] H. C. Casey, Jr. and F. Stern, J. Appl. Phys. **47**, 631 (1976).

[34] J. Serre, A. Ghazali, and P. Leroux Hugon, Phys. Rev. B **23**, 1971 (1983).

[35] J. Serre and A. Ghazali, Phys. Rev. B **28**, 4704 (1983).

[36] K.-F. Berggren and B. E. Sernelius, Phys. Rev. B **24**, 1971 (1981).

[37] T. S. Moss, Proc. Phys. Soc. London, Sect. B **67**, 775 (1954); E. Burstein, Phys. Rev. **93**, 632 (1954).

[38] D. B. Haddad, J. S. Thakur, V. M. Naik, G. W. Auner, R. Naik, and L. E. Wenger, in *GaN and Related Alloys*, MRS Symposia Proceedings No. 743, edited by C. Wetzel, E. T. Yu, J. S. Speck, A. Rizzi, and Y. Arakawa (Materials Research Society, Warrendale, PA, 2003), p. L111.22.

[39] V. M. Naik, R. Naik, D. B. Haddad, J. S. Thakur, G. W. Auner, H. Lu, and W. J. Schaff, Appl. Phys. Lett. **86**, 201913 (2005).

[40] C. Stampfl, C. G. Van de Walle, D. Vogel, P. Kruger, and J. Pollmann, Phys. Rev. B **61**, R7846 (2000); S. Limpojumnong and C. G. Van de Walle, Phys. Status Solidi B **228** 302 (2001).

[41] T. L. Tansley and R. J. Egan, Phys. Rev. B **45**, 10942 (1992).

[42] See, for example, G. H. Wannier, *Elements of Solid State Theory* (Cambridge University Press, Cambridge, England, 1959), p. 212.

[43] D. Fritsch, H. Schmidt, and M. Grundmann, Phys. Rev. B **67**, 235205 (2003).

[44] Y. C. Yeo, T. C. Chong, and M. F. Li, J. Appl. Phys. **83**, 1429 (1998).

[45] S. K. Pugh, D. J. Dugdale, S. Brand, and R. A. Abram, Semicond. Sci. Technol. **14**, 23 (1999).

[46] Y. Ishitani *et al.*, Phys. Status Solidi B **241**, 2849 (2004).

[47] I. Hamberg, C. G. Granqvist, K.-F. Berggren, B. E. Sernelius, and L. Engstrom, Phys. Rev. B **30**, 3240 (1984).

[48] C. F. Ting, T. K. Lee, and J. J. Quinn, Phys. Rev. Lett. **34**, 870 (1975).

[49] T. M. Rice, Ann. Phys. (N.Y.) **31**, 100 (1965).

[50] L. Hedin, Phys. Rev. **139**, A796 (1965); J. J. Quinn and R. A. Ferrell, *ibid.* **112**, 812 (1958).

[51] N. E. Christensen and I. Gorczyca, Phys. Rev. B **50**, 4397 (1994).

[52] Y.-N. Xu and W. Y. Ching, Phys. Rev. B **48**, 4335 (1993).

[53] D. Pines and P. Nozieres, *The Theory of Quantum Liquids* (Benjamin, New York, 1966), Vol. I.

[54] S. DasSarma, V. M. Galitski, and Y. Zhang, Phys. Rev. B **69**, 125334 (2004).

[55] A. A. Abrikosov, L. P. Gorkov, and I. E. Dzyaloshinski, *Methods of Quantum Field Theory in Statistical Physics* (Prentice-Hall, Englewood Cliffs, NJ, 1963), Sec. 39.

[56] G. D. Mahan, *Many-Particle Physics*, 3rd ed. (Plenum, New York, 2000), Chap. 7.

[57] G. D. Mahan, *Many-Particle Physics*, 3rd ed. (Plenum, New

York, 2000), p. 199.
[58] C. Bungaro, K. Rapcewicz, and J. Bernholc, Phys. Rev. B **61**, 6720 (2000).
[59] C. Persson, R. Ahuja, A. F. da Silva, and B. Johansson, J. Appl. Phys. **92**, 3207 (2002).
[60] D. Fritsch, H. Schmidt, and M. Grundmann, Phys. Rev. B **67**, 235205 (2003).
[61] J. Wu, W. Walukiewicz, W. Shan, K. M. Yu, J. W. Ager III, S. X. Li, E. E. Haller, H. Lu, and W. J. Schaff, J. Appl. Phys. **94**, 4457 (2003).
[62] J. Edwards, K. Kawabe, G. Stevens, and R. J. Tredgold, Solid State Commun. **3**, 99 (1965).
[63] M. Morita, K. Tsubouchi, and N. Mikoshiba, Jpn. J. Appl. Phys., Part 1 **21**, 728 (1982).
[64] G. A. Cox, D. O. Cummings, K. Kawabe, and R. H. Tredgold, J. Phys. Chem. Solids **28**, 543 (1968).
[65] R. W. Francis and W. L. Worrell, J. Electrochem. Soc. **123**, 430 (1976).
[66] A. G. Bhuiyan, A. Hashimoto, and A. Yamamoto, J. Appl. Phys. **94**, 2779 (2003).